IEEE Access
Multidisciplinary | Rapid Review | Open Access Journal

Received December 1, 2019, accepted January 14, 2020, date of publication January 23, 2020, date of current version January 31, 2020.

Digital Object Identifier 10.1109/ACCESS.2020.2968967

Noninvasive Classification of Blood Pressure Based on Photoplethysmography Signals Using Bidirectional Long Short-Term Memory and Time-Frequency Analysis

HENDRANA TJAHJADI, (Member, IEEE), KALAMULLAH RAMLI, (Member, IEEE), AND HENDRI MURFI

Department of Electrical Engineering, Universitas Indonesia, Depok 16424, Indonesia

Corresponding author: Kalamullah Ramli (kalamullah.ramli@ui.ac.id)

This work was supported by the Universitas Indonesia through the Q1Q2 International Journal Publication Grant Scheme under Contract NKB-0306/UN2.R3.1/HKP.05.00/2019.

ABSTRACT The photoplethysmography (PPG) method for continuous noninvasive measurements of blood pressure (BP) offers a more comfortable solution than conventional methods. The main challenge in using the PPG method is that its accuracy is greatly influenced by motion artifacts. In addition, the characteristics of PPG vary depending on physiological conditions; hence, the system must be calibrated to adjust for such changes. We attempt to address these limitations and propose a novel method for the classification of BP using a bidirectional long short-term memory (BLSTM) network with time-frequency (TF) analysis based on PPG signals. The TF analysis extracts information from PPG signals using a short-time Fourier transform (STFT) in the time domain to produce two features, namely, the instantaneous frequency and spectral entropy. Training the BLSTM network using TF features significantly improves the classification performance and decreases the training time. We classify 900 PPG waveform segment samples from 219 adult subjects into three classification levels: normotension (NT), prehypertension (PHT) and hypertension (HT). The results show that the proposed method is successful in the classification of BP with accuracy, sensitivity, and speciticity values of 97.33%, 100%, and 94.87%, respectively. The F1 scores of three BP classifications were 97.29%, 97.39%, and 93.93%, respectively. A comparison of current and previous approaches to the classification of BP is accomplished. Our proposed method achieves a higher accuracy than convolutional neural networks (CNNs), k-nearest neighbors (KNN), bagged tree, logistic regression, and AdaBoost tree methods.

INDEX TERMS Blood pressure, BLSTM, LSTM, photoplethysmography, PPG, time-frequency analysis.

I. INTRODUCTION

Blood pressure (BP) is an important parameter for the early detection of heart disease because it is associated with symptoms of hypertension or hypotension [1]. BP measures the power from the heart pump that is provided to artery walls when circulating throughout the body [2], [3]. The result of a BP measurement consists of three parameters, namely, the diastolic BP (DBP), systolic BP (SBP), and mean arterial pressure (MAP), in millimeters of mercury (mmHg) [4].

There are two types of methods for measuring BP: invasive and noninvasive methods. Although invasive methods have been known to be able to measure BP accurately and continuously, these methods are not very convenient to apply and trigger infections in patients [5]. The noninvasive methods that are currently implemented using a cuff cause discomfort, especially for wounded people, overweight people, and newborns [6], [7].

To simplify the measurement process and to make it more comfortable, noninvasive methods of measuring BP without cuffs, such as ballistocardiography (BCG), electronic bioimpedance (EBI), tonometry, and photoplethysmography (PPG), have been introduced [8].

The associate editor coordinating the review of this manuscript and approving it for publication was Michael Friebe.

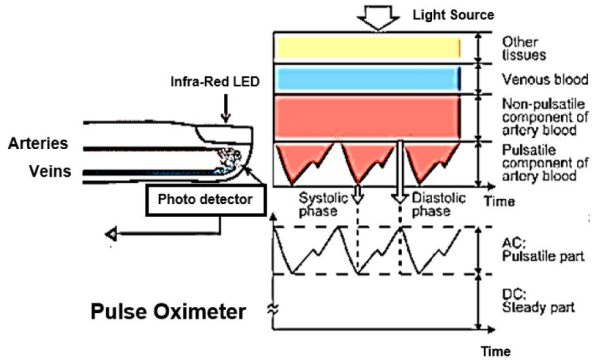

FIGURE 1. DC and AC components of the PPG signal due to variation in light absorption [23].

We currently focus on discussing the measurement of BP through PPG signals. A single PPG-based BP estimation study was conducted to make users more comfortable. The features of PPG are also known to carry important information that can be used as physiological parameters [9]. Our previous work has shown statistically that the features of PPG can be used to estimate BP [10]. The generation of PPG signals requires some optoelectronic components, namely, a light-emitting diode (LED) and a photodetector. An LED is a light source that can be used to illuminate blood vessels so that small perfusion changes can be monitored in the photodetector. Perfusion is measured as the rate at which blood is delivered to tissue. This mechanism is illustrated in Fig. 1. Despite the simplicity of this measurement technique, several potential sources of error exist in BP estimation methods based on PPG as follows:

1. The feature points of each PPG waveform need to be extracted precisely. The problem is that using too many features increases the computational complexity, and overfitting occurs [11].
2. The quality of the PPG signal is easily degraded by poor blood circulation, and the PPG waveform characteristics vary with changes in peripheral vascular resistance, blood vessel wall elasticity, and blood viscosity [12], [13]. The system must be calibrated to adjust for varying PPG waveform characteristics [13]–[15]. Therefore, the system requires frequent recalibrations for each person.
3. The PPG signal is easily affected by motion artifacts, leading to errors in the measurement. Most motion artifacts correlate with the sensor motion relative to the skin; therefore, optimized filtering is needed [16]–[18].

In this paper, we propose a novel classification method for BP based on PPG using bidirectional long short-term memory (BLSTM) with time-frequency (TF) analysis. Our main contributions are as follows:

1. Most previous studies have focused on the estimation of BP values. However, for these methods [19]–[21], a clinical reference is needed. We focus on a BP classification based on the Joint National Committee (JNC 7). With our proposed method, users can immediately know the condition of their BP.
2. There are two main problems in deep learning classification methods: classification accuracy and time consumption during training. Our proposed method uses BLSTM combined with TF analysis to achieve a faster training time. Training the BLSTM network using TF features significantly improves the classification performance and decreases the training time.
3. We use a method based on TF analysis to compensate for motion artifacts. With our proposed method, a special process is not needed to ensure the PPG signal quality.
4. We use BLSTM to compensate for BP instability, which eliminates the need for a calibration process.

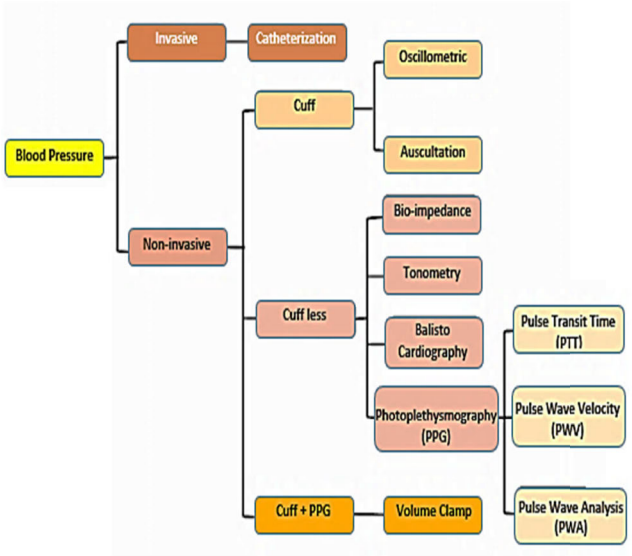

FIGURE 2. A map of research works for BP measurement methods. There are two types of methods for measuring BP: invasive methods and noninvasive methods. BP measurement methods based on PPG are divided into three groups: pulse transit time (PTT), pulse wave velocity (PWV) and pulse wave analysis (PWA) methods [8].

This paper is organized as follows. Section II describes the related work using different methods. Section III describes the methodology. The experimental results are given in section IV. Section V discusses the results. The conclusion is presented in section VI.

II. RELATED WORK

In this section, we discuss some of the studies and frameworks related to BP measurements based on PPG signals. A categorization of the current methods is shown in Fig. 2 [8].

A. BP ESTIMATION BASED ON PPG WITH A CUFF

The volume clamp method is still partly occlusive because it uses a small cuff around the finger. The device uses an inflatable finger cuff with a built-in PPG sensor, as illustrated in Fig. 3 [22]. A continuous measurement of BP is possible with the volume clamp but is still uncomfortable for patients.

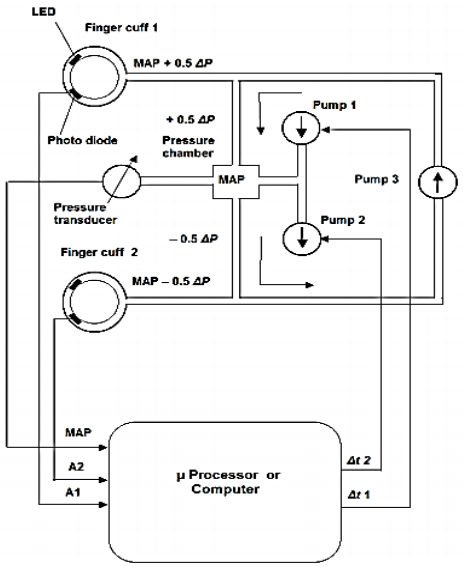

FIGURE 3. The feedback system assembled based on a microprocessor or computer is supplied with photoplethysmography signals A1 and A2 from inflatable finger cuffs 1 and 2. The latter compares the input signals and forms corresponding output signals as time intervals during which pump 1 (for increasing the pressure) or pump 2 (for decreasing the pressure) is active. To obtain the maxima of the shifted oscillometric envelopes, the constant airflow pump 3 is used to create a small pressure difference ΔP of a controlled value (approximately 30 mm Hg) between the cuffs. Thus, the counterpressures in cuffs 1 and 2 are kept equal to MAP + 0.5 ΔP and MAP − 0.5 ΔP, respectively. The pressure in the central point of the pneumatic circuit (in the pressure chamber) is equal to the MAP [22].

Variations in the finger positioning within the cuff influence the BP measurement, reducing its precision [8].

B. BP ESTIMATION BASED ON PPG WITHOUT A CUFF

The motivation behind this approach is to avoid frequent cuff-based BP measurements, which cause significant discomfort to the patient. The methods are as follows:

1) PULSE WAVE VELOCITY METHODS

Pulse wave velocity (PWV) methods use signals from two PPG sensors at a known distance apart along the same arterial branch to calculate the velocity of the pulse wave, as shown in Fig. 4. The pressure is measured by the difference between the pulse transit time (PTT) of the previous sensor and the pulse time at the leading sensor [8]. The peripheral PWV can then be determined from the transit time and transit distance. Unfortunately, finding an arterial location requires a trained medical expert. The distance between the two PPG signals used to determine the arrival time must be measured precisely and manually and requires calibration. The accuracy is significantly affected by motion during the BP measurement. The PWV has become an important parameter in BP analysis [23]–[25]. The evaluation of the BP value from the PWV can be described by Equation (1). The relationship between the vessel elasticity and the wave speed of a pressure pulse in a thin-walled vessel can be described by the Moens-Kortweg

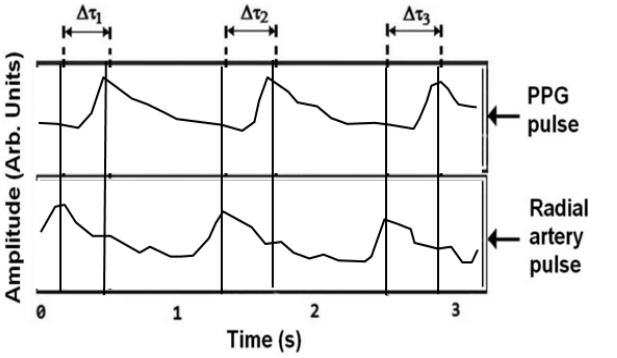

FIGURE 4. PWV method uses signals from two PPG sensors separated by a known distance (D) along the same arterial branch and Δ_T (PTT) to calculate the velocity of the pulse wave [8].

Equation [23]:

$$PWV = \frac{\boldsymbol{D}}{PTT^2} = \sqrt{\frac{hE_0 exp^{(\zeta P)}}{\rho R}} \tag{1}$$

where PWV is the pulse wave velocity, D is the length of the vessel, PTT is the pulse transit time, h is the thickness of the vessel wall, R is the radius of the vessel, ζ is the blood density, E_0 is the zero-pressure modulus in mmHg, and ρ is a constant that depends on the particular vessel (typically 0.016 $mmHg^{-1}$ to 0.018 $mmHg^{-1}$).

2) PULSE TRANSIT TIME METHODS

The most common approach for noninvasive, cuffless BP measurements is PTT-based techniques. PTT-based techniques involve measurement of the transit time of blood between two points in the body [26]. PTT-based techniques use signals from electrocardiography (ECG) and PPG. The PTT is the time delay associated with the pressure wave traveling between two arterial sites, as shown in Fig. 5. The evaluation of the BP value from the PTT can be described by Equation (2) [27].

$$SBP = A \times l_n \frac{r}{PTT^2} + B \tag{2}$$

SBP is the systolic BP, PTT is the pulse transit time, and r is the diameter of the blood vessels. The values of the constants A and B depend on the elasticity of the arteries.

3) PULSE WAVE ANALYSIS METHODS

Currently, there are two ways to achieve BP estimation using only PPG. The first approach is a parametric model that attempts to extract certain parameters such as the systolic, heart rate, and diastolic periods from each PPG signal. BP estimation can be achieved using these parameters [23]. Some examples of parametric methods include regression of long-term and short-term features [28], the pulse transport theory-based model [29], linear regression [23], and the Windkessel model [30]. The second element of the Windkessel model estimates the total peripheral resistance and determines the value of the body's arterial capacitance

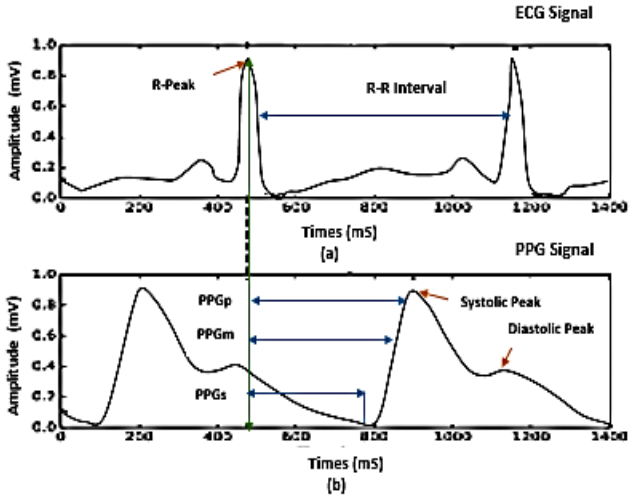

FIGURE 5. PTT-based techniques measure the transit time of blood between two points inside the body. PTT-based techniques use signals from ECG (a) and PPG (b). PTT features: PTT values are obtained by measuring the time interval between the ECG R-peak and three points on the PPG signal: the PPG maximum (PPGp), the PPG minimum (PPGm), and the point at which the maximum slope of the PPG waveform occurs (PPGs) [26].

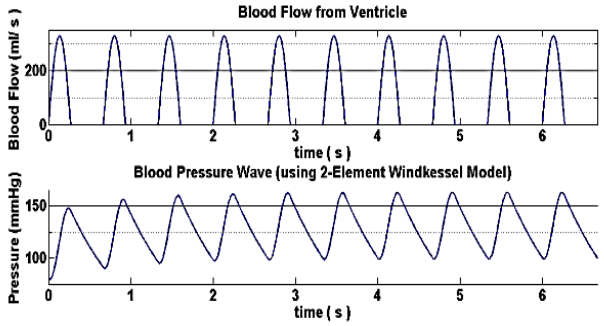

FIGURE 6. BP simulation using a 2-element Windkessel model for SBP/DBP = 160/100 mmHg and HR = 90 bpm parametric models [30].

through the PPG signal, as shown in Fig. 6. Parametric models can achieve good prediction results for an individual, but the accuracy decreases over time. Moreover, these models require an initial calibration and frequent recalibrations for each person.

The second approach involves nonparametric models, which try to extract specific features in the frequency domain or time domain, as shown in Fig. 7 [24]. The limitations of pulse wave analysis (PWA) methods are as follows:

1. PWA methods reduce the hardware complexity for cuffless BP estimation, but the accuracy is significantly affected by motion artifacts during the BP measurement.
2. The feature points of each PPG waveform need to be extracted correctly, and the PPG signals must be of high quality [31]. A comparison of the existing BP estimation methods is shown in Table 1.

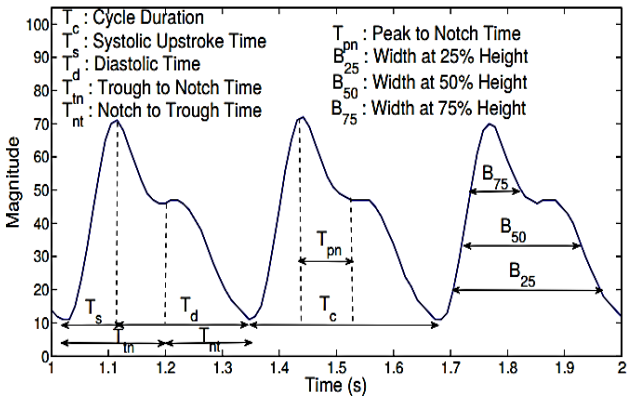

FIGURE 7. The PPG features commonly used in prior studies related to BP are the cycle duration (Tc), systolic time (Ts), diastolic time (Td), trough to notch time (Ttn), notch to trough time (Tnt), peak to notch time (Tpn), and the sum of the systolic and diastolic widths at 25% (B25), 33% (B33), 50% (B50) and 75% (B75) of the signal amplitude in each cycle [24].

C. BP CLASSIFICATION BASED ON PPG

Blood pressure classification methods can automatically diagnose BP symptoms. Users can immediately know their BP condition, which provides an early warning system for potential patients. Visvanathan *et al.* [32] used a support vector machine (SVM) to classify BP values. The classification process was performed using the radial basis function (RBF) kernel. They divided the BP value range into bins consisting of hypotension, desired, prehypertension stage 1 hypertension stage 2 hypertension, and hypertensive. Their proposed method with frequency domain features was first tested with The University of Queensland vital signs dataset, which covers a wide range of BP values, recorded from 32 surgical cases ranging in duration from 13 minutes to 5 hours over a period of 4 weeks at the Royal Adelaide Hospital.

In recent years, deep learning techniques have shown their outstanding performance in pattern recognition applications. Liang *et al.* [33] examined in-depth learning methods for classifying BP based on PPG signals using a continuous wavelet transform (CWT) and convolutional neural networks (CNNs). To classify BP based on PPG signals, three classification experiments were conducted. The study used 80% of the dataset for training and the remaining 20% for testing. The F1 scores for the normotension (NT) group vs prehypertension (PHT) group, NT and PHT groups vs hypertension (HT) group, and NT group vs HT group were 72.97%, 81.82%, and 92.31%, respectively.

III. METHODOLOGY

We propose a novel method for classifying BP using BLSTM networks with TF analysis based on a PPG signal, as shown in Fig. 8. Original PPG signals were shared from the PPG-BP figshare database [34]. We divided the data into signal and label groups. The signals were a cell array consisting of a collection of PPG signals. The labels were an array of categories that contained the ground-truth labels from the signals. Then, we split the signal group into a training set to train the classifier and a test set to test the accuracy of the classifier.

TABLE 1. Comparison of PPG methods with existing BP measurement methods.

No.	Methods	Measurement	Accuracy	Sensors Used	Medical Supervision	Calibration
1	Auscultatory [5]	Discrete time	Gold standard for clinical applications	Cuff	Yes	Never
2	Oscillometric [2]	Discrete time	Gold standard for automatic mode	Cuff	Yes	Never
3	Volume clamp [29]	Discrete time	Controversial	Finger Cuff + PPG	Yes	Never
4	PWV [24]	Continuous	Controversial	PPG (wrist) + PPG (finger)	Yes	Yes
5	PTT [27]	Continuous	Controversial	ECG + PPG (finger)	Yes	Yes
6	PWA [30]	Continuous	Controversial	PPG (finger)	Yes	Yes

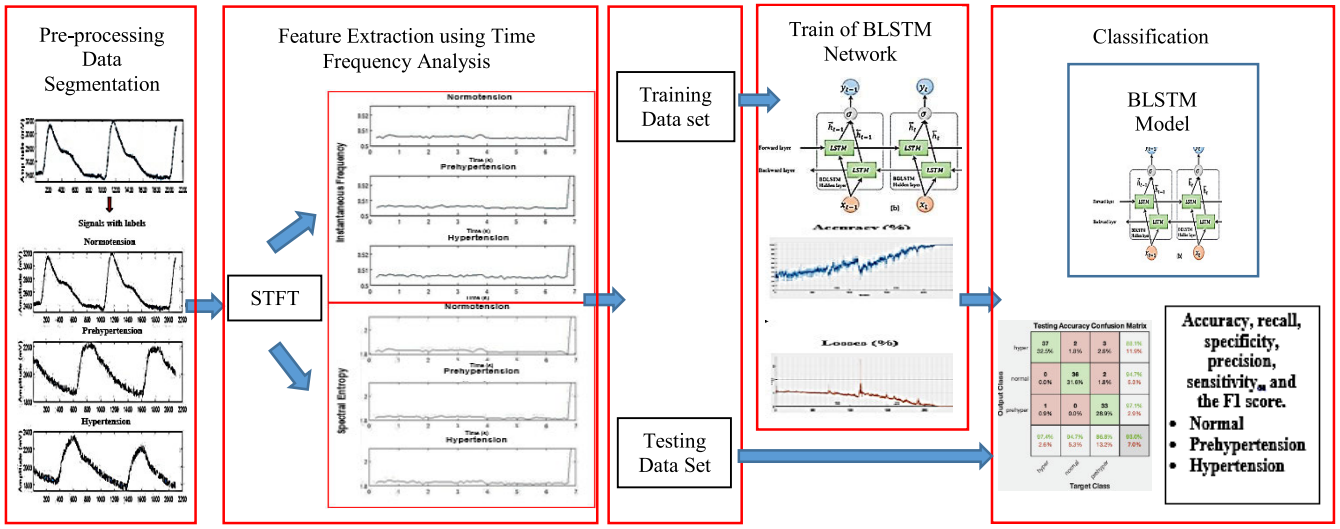

FIGURE 8. Detailed block diagram of the proposed BP classiïĄcation technique. The four blocks represent the processing steps: pre-processing (data segmentation), feature extraction, training of the network and the results of classification. During the data segmentation phase, the skewness signal quality index (SSQI) value is recorded for each PPG segment for a particular subject. In this phase, to prevent bias, dataset balancing is used by duplicating signal data at each level of classification so that each group has the same number of datasets, namely 300 normotensive subjects, 300 prehypertensive subjects, and 300 hypertensive subjects. Each PPG waveform was subsequently transformed into the instantaneous frequency and spectral entropy using a short-time Fourier transform (STFT) with 63 windows. In this study, the dataset includes 786 subjects in the training set and 114 subjects in the testing set. Each time frequency moment can be used as a one-dimensional feature as input to BLSTM. Finally, BLSTM classiïĄers are used to classify the BP.

The input one-dimensional PPG time domain was divided into BP levels for adults in three main categories, normotension (NT), prehypertension (PHT), and hypertension (HT), according to the BP levels in the JNC 7 report. Waveforms of the PPG signals are shown in Fig. 9. In this phase, to prevent bias, dataset balancing (hold up methods) was used by duplicating signal data at each level of classification until each group had the same number of datasets (300 normal subjects, 300 PHT subjects, and 300 HT subjects). In this study, the dataset has 786 subjects for the training set and 114 subjects for the testing set. There are five processing steps: pre-processing (data segmentation), feature extraction using time frequency analysis, training of the network and the results of classification.Each moment Time frequency moment can be used as a one-dimensional feature as input to the BLSTM networks. In this study, a confusion matrix is used to visualize classifier performance for a set of data where the true values are known. To comprehensively evaluate the

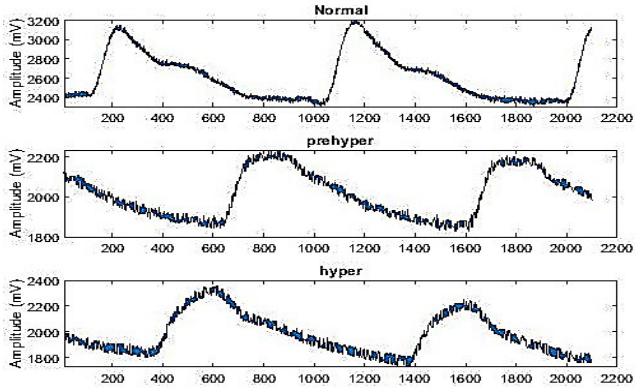

FIGURE 9. Three different BP classifications. Each segment consists of 2100 sampling points, corresponding to 2.1 s of data.

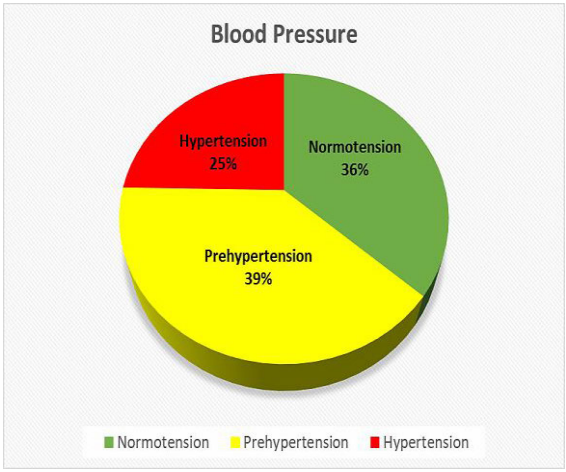

FIGURE 10. Pie chart of dataset BP subjects.

testing models, various evaluation indices were used, including accuracy (Ac), recall (Re), specificity (Sp), precision (Pr), sensitivity (Se), and the F1 score.

A. DATA ACQUISITION

The dataset was collected from 219 adult subjects aged 21–86 years. Males accounted for 48% of the participants. We collected 900 recorded data values from the PPG-BP figshare database [34]. A dataset collection program was written to obtain information about individual basic physiology and collected PPG waveform signals and detected the arterial BP at the same time. The dataset includes PPG and BP information from subjects who were diagnosed with NT, PHT, and HT, as detailed in Fig. 10. The records include an identification number, sex, age, and disease. The total duration of the experiment was approximately 15 min. The data collected from the PPG signals and BP took approximately 3 min. Each data segment consisted of 2100 sampling points, which corresponded to 2.1 s of data. The waveform was sampled at a frequency of 1 kHz during the signal acquisition, with a 12-bit analog-to-digital conversion precision.

Each individual was asked to sit in an office chair in their most comfortable posture and to relax their arms on an empty desk. Each individual had 10 min to adapt to the environment and adjust their breathing after entering the data collection room [34]. The specific collection settings were as follows: The PPG signal was collected at the fingertip of the left index finger, and the arterial BP was collected from the right forearm. The arterial BP measurement was performed by a hospital nurse.

Before the participant record was archived, a data integrity screening, data availability screening and signal quality evaluation (to remove abnormal and high-noise data) were required to be conducted to form a high-quality dataset. The detailed process of inclusion and exclusion is described as follows [34]:

1. Data integrity screening: This procedure incorporates the screening of absent and unusual qualities of essential physiological data, disease information, BP, heart rate, and 3 sections of waveform information. If one or more items were missing or if there was an abnormal value, the participant record was removed.
2. Data availability screening: This dataset is designed to focus on clinical information for cardiac vascular diseases (CVDs) and other closely related diseases, such as diabetes. Data from CVD patients who were diagnosed with non-CVD diseases (except diabetes) were excluded during the screening process to ensure that the dataset only contains data from participants who were diagnosed with the disease of interest.
3. Waveform signal quality evaluation: All 3 sections for each participant underwent a signal quality evaluation and a robust signal quality index (SQI) method was applied to achieve this step. If the SQIs of the 3 sections for one subject were lower than the mean SQI calculated from the sections of all subjects, the subject data were removed.

The waveform signal quality evaluation method adopted the skewness signal quality index (SSQI) [34]. Orphanidou [35] found that skewness is associated with corrupted PPG signals and has a certain connection with the quality of PPG signals. Liang *et al.* [36] found skewness to be the optimal method for assessing the SQI in PPG signals. Skewness characterizes the degree of asymmetry of a given distribution around its mean. If the distribution of the data is symmetric, then the skewness will be close to 0. Positive skewness indicates a distribution with an asymmetric tail extending toward more positive values. Negative skewness indicates a distribution with an asymmetric tail extending toward more negative values, as shown in Fig. 11 [37]. Each segment of the PPG signal was evaluated by classification thresholds as an excellent, acceptable, or unfit PPG waveform to determine whether it should be saved, as detailed in Fig. 12 [38]. This step was developed to reduce the PPG segments with high noise and motion artifacts. Skewness is used to measure the probability distributions of symmetric

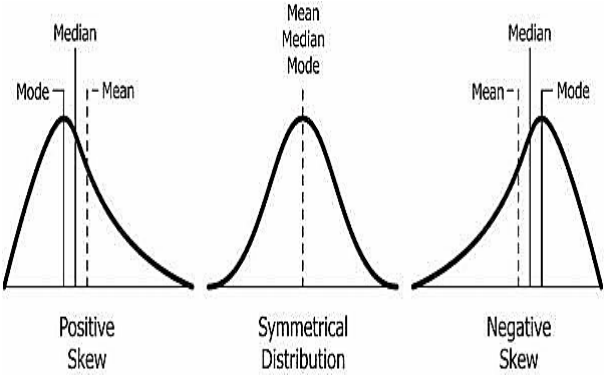

FIGURE 11. Illustration of skewness.

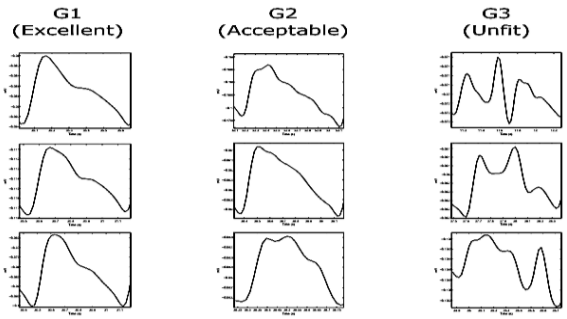

FIGURE 12. The PPG waves were categorized into three categories: G1 contains beats with clear systolic and diastolic waveforms with dicrotic notches; G2 contains beats without clear systolic and diastolic waveforms and without dicrotic notches; and G3 contains noisy waveforms [38].

signals. Mathematicians discuss skewness in terms of the third moment around the mean. The specific definition is as follows [37]:

$$S_{SQI} = \frac{\sum_{i=1}^{N}(A_i - \bar{A})^3}{(N-1) * \sigma^3} \tag{3}$$

where S_{SQI} is the skewness signal quality index, N is the number of variables in the distribution, σ is the standard distribution, A_i is a random variable, and $\bar{A}$ is the mean of the distribution.

B. PPG DATA PREPROCESSING

A PPG signal is a nonstationary signal similar to other biomedical signals. This means that the frequency and bandwidth can vary with time. To overcome the disadvantages of nonstationary signals, nonstationary methods such as frequency analysis are needed [39]. TF analysis is an effective tool for understanding the nonstationary and nonlinear nature of a signal [40]. In this phase, data exploration is carried out using a spectrogram to visually determine the shape of the PPG signal according to its BP classification as well as to observe the amount of noise contained in the PPG signal. As shown in Fig. 13, the data exploration process is not included in the main process; therefore, this process is not included in the methodology block diagram that refers to Fig. 8.

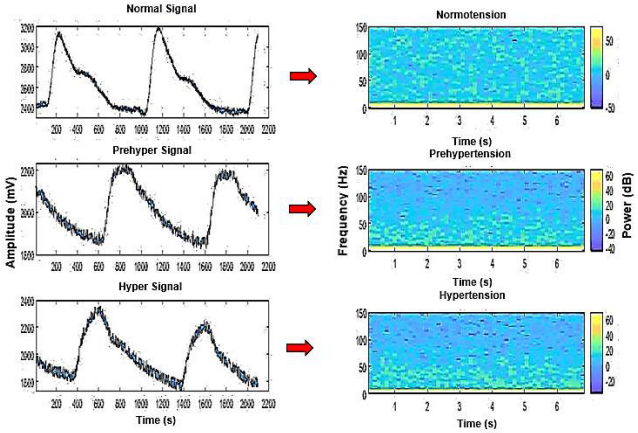

FIGURE 13. PPG spectrograms belonging to each class of BP.

C. FEATURE EXTRACTION

The process of extracting features from data can help improve the accuracy of training and testing of the classifier. The TF moment extracts information from the PPG signals using a STFT into two TF moments in the time domain, instantaneous frequency and spectral entropy, as shown in Fig. 14.

The instantaneous frequency function estimates the time-dependent frequency of a signal at the first moment of the power spectrogram. The instantaneous frequency of a real-time signal is defined as [41]:

$$FI\,(t) = \frac{1}{2\pi}\frac{d}{dt}\emptyset(t) \tag{4}$$

where FI is the instantaneous frequency and $\emptyset(t)$ is the instantaneous phase of the analytic signal associated with the real-time signal.

Subtle changes in the characteristics of PPG signals in the time domain cannot be observed by the human eye. Therefore, it is necessary to use methods to extract time- or frequency-domain features [42]. One such feature of interest is entropy. Spectral entropy can provide detailed information about the signal complexity based on the spectrum width. A high entropy is associated with a wider spectrum, such as in the case of white noise, and a narrow spectrum reflects a low entropy, such as in the case of a sum of sinusoids. In fact, the spectral entropy calculates information that is included in the various frequency components. The following equation is used to compute the spectral entropy:

$$P(\omega_i) = \frac{1}{N}\,|X(\omega_i)|^2 \tag{5}$$

$$P_i = \frac{P(\omega_i)}{\sum_i (\omega_i)} \tag{6}$$

$$PSE = -\sum_{i=1}^{n} P_i \ln P_i \tag{7}$$

where $P(\omega_i)$ is the power spectral density, $X\,(\omega_i)$ is the spectrum of the signal, N is the number of points in the spectrum, P_i is the probability density function, and PSE is the power spectral entropy. In this study, the spectral entropy uses 63 time windows to compute the spectrogram. The entropy

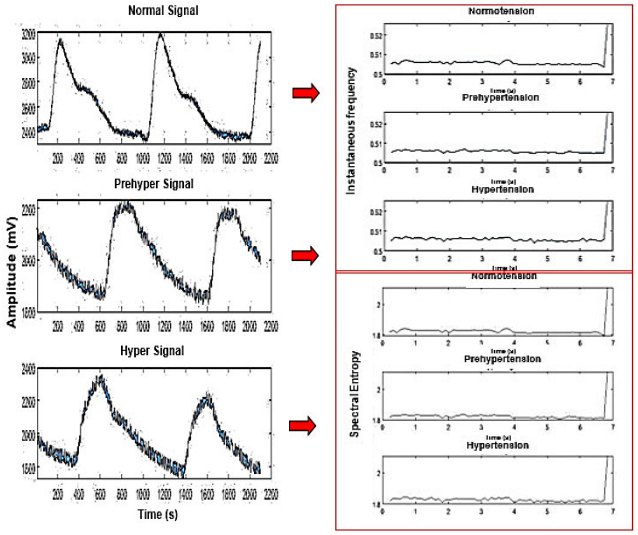

FIGURE 14. Instantaneous frequency and spectral entropy from each PPG signal.

for each time window is computed from x by [43]:

$$H = -\sum_{i=1}^{N} x_{\mathrm{i}}\, log_2 x_{\mathrm{i}} \tag{8}$$

where x_{i} is the probability mass function spectrum of the signal and N is the number of points in the spectrum.

D. BIDIRECTIONAL LONG SHORT-TERM MEMORY

BLSTM is widely used to solve several classification problems related to sequential data and has become a state-of-the-art classifier [20]. The long short-term memory (LSTM) layer can process a time series only in one direction (forward), whereas a BLSTM layer processes the time series in both directions (forward and backward) [44]–[49]. The hidden layer of LSTM is also named an LSTM cell, as shown in Fig. 15a [44]. At time t, the input gate, forget gate, output gate, layer input, layer output, cell input state, cell output state, and previous cell output state are denoted as $it, f_{\mathrm{t}}, o_{\mathrm{t}}, x_t, h_t, \check{C}_t, C_t$, and C_{t-t}, respectively [44]. The input gate, forget gate,, forget gate, output gate, and cell input state can be calculated using the following Equations [44]:

$$f_{\mathrm{t}} = \sigma_{\mathrm{t}}\left(W_{\mathrm{p}} x_{\mathrm{t}} + U_{\mathrm{p}} h_{\mathrm{t-1}} + b_{\mathrm{p}}\right) \tag{9}$$

$$i_{\mathrm{t}} = \sigma_{\mathrm{t}}\left(W_{\mathrm{i}} x_{\mathrm{t}} + U_{\mathrm{i}} h_{\mathrm{t-1}} + b_{\mathrm{i}}\right) \tag{10}$$

$$o_{\mathrm{t}} = \sigma_{\mathrm{t}}\left(W_{\mathrm{o}} x_{\mathrm{t}} + U_{\mathrm{o}} h_{\mathrm{t-1}} + b_{\mathrm{o}}\right) \tag{11}$$

$$\check{\mathrm{C}}_{\mathrm{t}} = tanh\left(W_{\mathrm{e}} x_{\mathrm{t}} + U_{\mathrm{e}} h_{\mathrm{t-1}} + b_{\mathrm{e}}\right) \tag{12}$$

where W_{p}, W_{i}, W_{o}, and W_{e} are the weight matrices mapping the hidden layer input to the three gates and the input cell state; U_{p}, U_{i}, U_{o}, and U_{e} are the weight matrices connecting the previous cell output state to the three gates and the input cell state; b_{p}, b_{i}, b_{o}, and b_{e} are four bias vectors; σ_{t} is the gate activation function, which normally is the sigmoid function; and *tanh* is the hyperbolic tangent function. Based on the results of the four above equations, at each time iteration t,

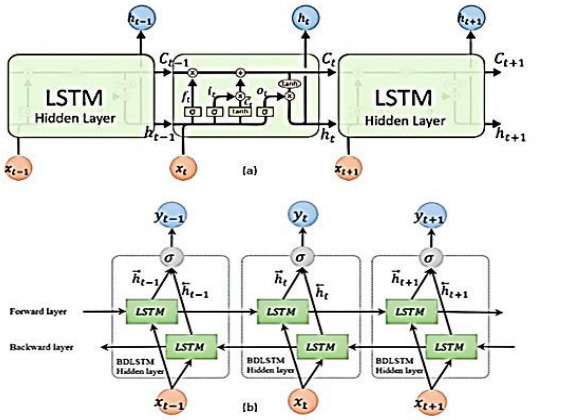

FIGURE 15. (a) Hidden layer of LSTM architecture. (b) BLSTM consists of two LSTM layers.

TABLE 2. Layer arrays.

No.	Layer architecture	Option
1st	Input sequence size	Sequence input with 2 dimensions
2nd	BLSTM	BLSTM with 100 hidden layers
3rd	Fully connected	3 fully connected layers
4th	Softmax	Softmax
5th	Classification output	Cross-entropy

the cell output state, $\check{\mathrm{C}}$, and the layer output, h, can be calculated as follows [44]:

$$C_{\mathrm{t}} = f_{\mathrm{t}} * C_{\mathrm{t}}^{-1} + i_{\mathrm{t}} * \check{\mathrm{C}} \tag{13}$$

$$h_{\mathrm{t}} = o_{\mathrm{t}} * \tanh C_{\mathrm{t}} \tag{14}$$

The final output of an LSTM layer should be a vector of all the outputs, represented by $\boldsymbol{Y}_t = [h_{1-\mathrm{n}}, \ldots, h_{\mathrm{t-1}}]$. To process the data, the first LSTM layer reads data from left to right, whereas the second LSTM layer reads data from right to left, as shown in Fig. 15.

E. BIDIRECTIONAL LONG SHORT-TERM MEMORY ARCHITECTURE

In this study, we use a BLSTM layer with an output size of 100 and output the last element of the sequence. We determine five layers, including the fully connected layer, followed by the softmax layer and the cross-entropy, as illustrated in Table 2.

IV. RESULTS

We conducted an experiment in MATLAB (R2019a version) to classify BP based on PPG signals using BLSTM networks with TF analysis. There are two main problems of deep learning classification methods: classification accuracy and

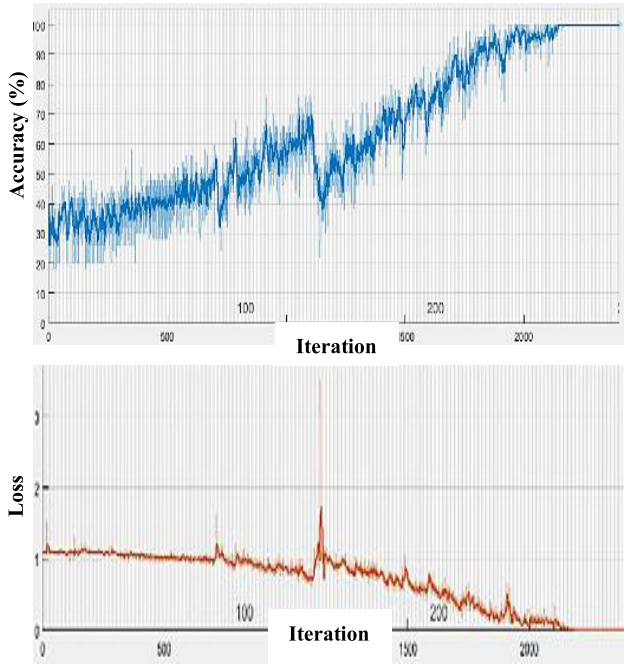

FIGURE 16. Training performance of BLS.

time consumption during training. Therefore, to evaluate the training performance in this study, a comparative analysis was conducted with the BLSTM model, GoogLeNet model, AlexNet model, and BLSTM model with TF analysis for the same dataset. We compared the training performance based on training time. We found that the training of a BLSTM network that uses PPG features required a very long time. The results indicate that our proposed method (BLSTM with TF analysis) achieves better training performance than the other classification methods, as shown in Table 3.

Referring to Fig. 16, for our proposed method (BLSTM with TF analysis), the top subplot of the training progress plot represents the training accuracy, and the value approaches 100%. The bottom subplot section represents the loss of the training, and the value of the loss in cross-entropy training in each mini-batch decreases to zero. This means that the training progresses successfully. The detailed parameter sets are shown in Table 4. The training process continues for as many as 300 epochs, allowing the network to make 300 passes through the training data. The initial learning rate is 0.01, which helps speed up the training process. We use a sequence length of 1000 to divide the signal into small pieces. Using this approach uses less memory even though more data are processed at one time. This study uses the adaptive moment estimation (ADAM) solver, which performs well for RNNs.

In this study, a confusion matrix is used to visualize classifier performance for a set of data where the true values are known. The confusion matrix from the training values are known. The confusion matrix from the training process of the BLSTM network is shown in Fig. 17. The axis labels are the class labels NT, PHT, and HT. The output class represents

TABLE 3. Comparison of training performance.

Method	Feature Extraction	Training Time	Training Option
BLSTM	PPG feature	50 min 51 sec	30 epochs
GoogleNet	CWT scalogram	57 min 31 sec	20 epochs
AlexNet	CWT scalogram	46 min 55 sec	20 epochs
BLSTM with TF analysis (proposed method)	STFT spectrogram	30 min 26 se	300 epochs

TABLE 4. Parameters of BLSTM network.

Setting Items	Detail
Input sequence size	2
Fully connected layer	3
Gradient threshold	1
Initial learning rate	0.01
Iterations per epochs	8
Maximum number of epochs	300
Maximum iterations	2400
Adaptive learning rate optimization	Adam

the label assigned to the signal by the network. The target class represents the ground-truth label of the signal. The green cells represent true positive (TP) or true negative (TN) signals, and the red cells represent false positive (FP) or false negative (FN) signals. The light gray cells provide row and column summaries. The bottom-right cell displays the overall accuracy. The confusion matrix of the training process shows that 100% of the ground-truth normal signals are correctly classified as NT, 100% of the ground-truth prehyper signals are correctly classified as PHT and 100% of the ground-truth hyper signals are correctly classified as HT. Furthermore, 100% of the normal signals are classified as NT, 100% of the prehyper signals are classified as PHT, and 100% of the hyper signals are classified as HT. The average training accuracy is 100%.

The confusion matrix of the testing process shows that 94.70% of the ground-truth normal signals are correctly classified as NT, 86.8% of the ground-truth prehyper signals are correctly classified as PHT, and 97.4% of the ground-truth hyper signals are correctly classified as HT Furthermore, 94.70% of the signals classified as NT are actually normal, 97.1% of the signals classified as PHT are actually prehyper, and 88.1% of the signals classified as HT are actually hyper. The average testing accuracy is 93.0%. The confusion matrix from the testing process of the BLSTM network is shown in Fig. 18.

TABLE 5. Classification performance of BLSTM with TF analysis.

Trial	TP (subjects)	FP (subjects)	TN (subjects)	FN (subjects)	Accuracy (%)	Sensitivity (%)	Specificity (%)	Recall (%)	Precision (%)	F1 Score (%)
Normotension (NT)	36	2	70	2	96.36	94.73	97.22	94.73	94.73	94.73
Prehypertension (PHT)	33	5	73	1	94.64	97.05	93.58	97/05	85.84	92.16
Hypertension (HT)	37	1	69	5	94.64	88.095	98.57	88.09	98.57	93.03
NT vs PHT	36	0	33	2	97.18	94.73	100.00	94.73	100.00	97.29
NT vs HT	36	2	37	0	97.33	100.00	94.87	100.00	94.73	97.29
(NT + PHT) vs HT	69	5	37	3	92.98	95.83	88.09	95.83	93.24	93.93

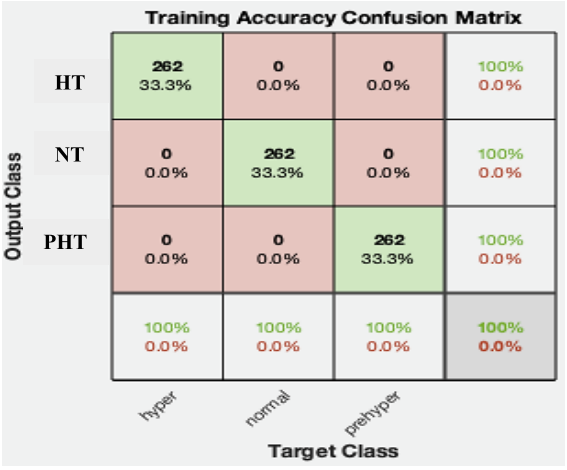

FIGURE 17. A training accuracy confusion matrix is used to describe the performance of the classifier in a dataset where the actual values are known.

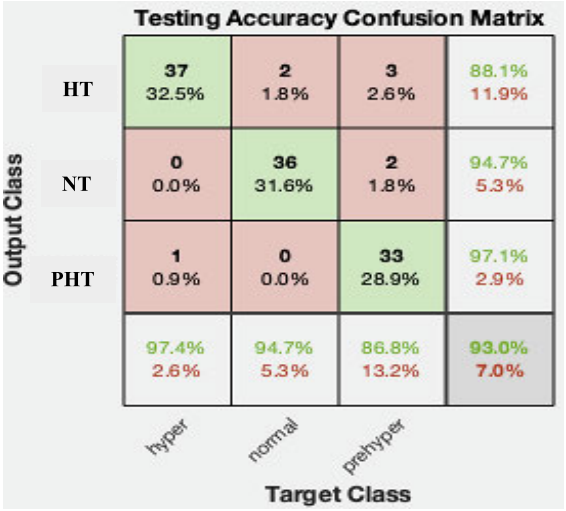

FIGURE 18. A testing accuracy confusion matrix is used to describe the performance of the classifier in a dataset where the actual values are known.

To comprehensively evaluate the testing models, various evaluation indices were used, including TP, FP, TN, FN, Ac, Re, Sp, Pr, Se, and the F1 score. The confusion matrix used for evaluating the classification performance is as follows [49]:

$$Ac = \left(\frac{Tp + Tn}{Tp + Fp + Tn + Fn}\right)100\% \tag{15}$$

$$Re = \left(\frac{Tp}{Tp + Fn}\right)100\% \tag{16}$$

$$Sp = \left(\frac{Tn}{Fp + Tn}\right)100\% \tag{17}$$

$$Se = \left(\frac{Tp}{Tp + Fn}\right)100\% \tag{18}$$

$$Pr = \left(\frac{Tp}{Fp + Tp}\right)100\% \tag{19}$$

$$F1 = \frac{2(Re \times Pr)}{(Re + Pr)} \tag{20}$$

where Ac is the accuracy, Re is the recall, Sp is the specificity, Se is the sensitivity, Pr is the precision, and F1 is the F1 score. The above six formulas are computed by the TP, FP, TN, and FN quantities. Table 5 shows the classification performance of our proposed method (BLSTM with TF analysis).

We performed a comparative study between our method and the results of previous studies. Table 6 presents a performance comparison with previous studies. To compare BP classifications based on a PPG signal, three classification experiments were carried out, NT vs PHT, NT vs HT, and NT vs (PHT + HT)). The first study [50] used the pulse arrival time (PAT) extracted from ECG, PPG signals, and PPG morphology features extracted from PPG. The study employed four distinctive classifiers: a bagged tree, k-nearest neighbors (KNN), logistic regression and an AdaBoost tree. These classifiers represent different classification methods, such as a bagged decision tree, regression, a decision tree, and

TABLE 6. Classification performance comparison.

Method	Trial	Feature Extraction	Database	Classifier	F1
PAT and PPG features [50]	NT (46 subjects) vs PHT (41 subjects) NT (46 subjects) vs HT (34 subjects) NT + PHT (87 subjects) vs HT (34 subjects)	PAT and 10 PPG features	121 subjects (MIMIC database)	AdaBoost tree	74.67% 90.15% 79.71%
PPG features [50]	NT (46 subjects) vs PHT (41 subjects) NT (46 subjects) vs HT (34 subjects) NT + PHT (87 subjects) vs HT (34 subjects)	10 PPG features	121 subjects (MIMIC database)	AdaBoost tree	72.26% 80.11% 63.76%
PAT features [50]	NT (46 subjects) vs PHT (41 subjects) NT (46 subjects) vs HT (34 subjects) NT + PHT (87 subjects) vs HT (34 subjects)	PAT features	121 subjects (MIMIC database)	AdaBoost tree	66.88% 68.04% 53.19%
PAT and PPG features [50]	NT (46 subjects) vs PHT (41 subjects) NT (46 subjects) vs HT (34 subjects) NT + PHT (87 subjects) vs HT (34 subjects)	PAT and 10 PPG features	121 subjects (MIMIC database)	Bagged tree	83.88% 94.13% 88.22%
PPG features [50]	NT (46 subjects) vs PHT (41 subjects) NT (46 subjects) vs HT (34 subjects) NT + PHT (87 subjects) vs HT (34 subjects)	10 PPG features	121 subjects (MIMIC database)	Bagged tree	78.48% 84.98% 75.32%
PAT features [50]	NT (46 subjects) vs PHT (41 subjects) NT (46 subjects) vs HT (34 subjects) NT + PHT (87 subjects) vs HT (41 subjects)	PAT features	121 subjects (MIMIC database)	Bagged tree	66.95% 84.98% 75.32%
PAT and PPG features [50]	NT (46 subjects) vs PHT (41 subjects) NT (46 subjects) vs HT (34 subjects) NT + PHT (87 subjects) vs HT (34 subjects)	PAT and 10 PPG features	121 subjects (MIMIC database)	Logistic regression	63.92% 79.11% 62.26%
PPG features [50]	NT (46 subjects) vs PHT (41 subjects) NT (46 subjects) vs HT (34 subjects) NT + PHT (87 subjects) vs HT (34 subjects)	10 PPG features	121 subjects (MIMIC database)	Logistic regression	63.66% 67.94% 47.10%
PAT features [50]	NT (46 subjects) vs PHT (41 subjects) NT (46 subjects) vs HT (34 subjects) NT + PHT (87 subjects) vs HT (34 subjects)	PAT features	121 subjects (MIMIC database)	Logistic regression	56.85% 67.85% 52.38%
PAT features [50]	NT (46 subjects) vs PHT (41 subjects) NT (46 subjects) vs HT (34 subjects) NT + PHT (87 subjects) vs HT (34 subjects)	PAT and 10 PPG features	121 subjects (MIMIC database)	KNN	83.34% 94.84% 88.49%
PPG features [50]	NT (46 subjects) vs PHT (41 subjects) NT (46 subjects) vs HT (34 subjects) NT + PHT (87 subjects) vs HT (34 subjects)	10 PPG features	121 subjects (MIMIC database)	KNN	78.62% 86.94% 78.44%
PAT features [50]	NT (46 subjects) vs PHT (41 subjects) NT (46 subjects) vs HT (34 subjects) NT + PHT (87 subjects) vs HT (34 subjects)	PAT features	121 subjects (MIMIC database)	KNN	66.95% 68.10% 53.19%
Raw PPG signal [33]	NT (46 subjects) vs PHT (41 subjects) NT (46 subjects) vs HT (34 subjects) NT + PHT (87 subjects) vs HT (34 subjects)	Continuous wavelet transform (scalogram)	219 subjects (Figshare database)	CNNs	80.52% 92.55% 82.95%
Raw PPG signal (proposed method in this study)	NT (38 subjects) vs PHT (38 subjects) NT (38 subjects) vs HT (38 subjects) NT + PHT (76 subjects) vs HT (38 subjects)	Short-time Fourier transform (spectrogram)	219 subjects (Figshare database)	BLSTM with time-frequency analysis	97.29% 97.39% 93.93%

a clustering method [50]. The second study [33] employed a CWT and CNNs. Table 6 shows that the F1 scores of our proposed method (BLSTM with TF analysis) were higher than those of the CNN classifier and regression methods, such as the bagged tree, KNN, logistic regression and AdaBoost tree methods. This result indicates that our BLSTM with TF analysis method achieves higher accuracy than the CNN, propagation and regression methods.

V. DISCUSSION

Our proposed method has promising potential and exclusively uses raw PPG signals to replace the PPG morphology feature extraction process for BP classification. Ideally, a method for measuring BP should offer high accuracy and should not require calibration or medical supervision [51].

The human physiological state is always dynamic in time, which makes estimating physiological signals a dynamic estimation problem. Therefore, certain physiological signals cannot be estimated using only the signal history without the current physiological conditions. Considering the valuable information of a temporal sequence and the dynamic nature of physiological signals, BLSTM is applied in our proposed method. CNNs are able to learn a local response from temporal or spatial data but lack the ability to learn sequential correlations [48]. In contrast to CNNs, RNNs are specialized for sequential modeling but are unable to extract features in a parallel manner [48].

The main challenge associated with using PPG is the influence of noise artifacts. The accuracy is significantly affected by noise artifacts [52]. In this study, we used two methods to avoid motion artifacts. The first method was implemented during the data collection process, where the data were evaluated using the SSQI before being stored. The SSQI value was recorded for each PPG segment of a particular subject. Values greater than zero were stored, and if the value was less than zero, the application asked the user to remove the PPG signal.

The second method involved using a method based on TF analysis to compensate for noise artifacts. Using TF analysis to obtain the instantaneous frequency and spectral entropy has the advantage of spreading noise in the TF field, which results in better estimates of higher noise levels. Frequency analysis is performed by segmenting a PPG signal into short periods that are presented in the form of a spectrum in a sliding window. Each pixel corresponds to a frequency and a time and represents the power of the PPG signal.

In this study, we used raw PPG signals to classify BP into different categories. To improve the accuracy of the training and testing of BLSTM, feature extraction from PPG signals is needed. Therefore, the raw PPG signal is first converted through an STFT into a TF moment to extract the features. The use of an STFT is a logical choice due to its speed and ease of use [53].

Moreover, another problem is that the PPG wave characteristics vary with changes in the blood vessel wall elasticity, peripheral vascular resistance, and blood viscosity and can cause measurement errors. For this reason, the system must be calibrated to adjust for changes in the PPG characteristics [54]. BLSTM is a kind of RNN architecture with LSTM units as hidden units and effectively solves vanishing gradient and gradient explosion problems. BLSTM combines a forward hidden layer and a backward hidden layer. BLSTM not only can exploit the context for long periods of time but also has access to the context in both previous and future directions. Therefore, BLSTM does not require a calibration process to adjust for various PPG wave characteristics.

In previous studies using deep learning for BP classification, the training unfortunately took a very long time [33]. In this case, because the training set was large, the training process could take several minutes. When a network uses data with a large range of values and a large average, the learning process and convergence of the network can be slow [55]. TF analysis produced the instantaneous frequency and spectral entropy using STFT with 63 time windows. In this case, each dataset no longer contains 2.100 sample points but contains only 63 sample features. With a small training set, the training process could take only a few minutes.

To comprehensively evaluate the testing models, various evaluation indices were used, including Ac, Re, Sp, Se, Pr, and the F1 score. Precision is a better metric when the cost of an FP is high. Recall helps when the cost of an FN is high. The F1 score is an overall measure of a model's accuracy that combines the precision and recall. A good F1 score indicates that the system has low FP and FN rates.

An advantage of BLSTM techniques is that they are quite effective when used as a solution for classification problems, including BP classification. BLSTM networks have been widely used to eliminate the negative effects of an active process from the past and future caused by the presence of nonlinear physiological changes. Considering the advantages of BLSTM, we use it as the classifier for BP in this study. A disadvantage associated with BLSTM is that it is necessary to pay attention to the width of the window according to the area of use since a good time resolution and a good frequency resolution cannot be obtained at the same time. Therefore, the relationship among the time duration, frequency bandwidth, and window size is very important.

VI. CONCLUSION

Users can immediately know the condition of their BP to ensure early detection using our proposed method. This method can expedite the treatment process and reduce the risk of mortality. Training a BLSTM network using TF moments such as instantaneous frequency and spectral entropy significantly improves the classification performance and decreases the training time. Our proposed method does not require a high-quality PPG signal and does not require an extraction of PPG morphological features; therefore, the method can be easily applied in many situations. In general, normotension had the highest accuracy with a value of 96.34% and achieved the best F1 score, with a value of 94.73%, among the classification levels. The results show that the classification of normotension vs hypertension (NT vs HT) shows the best results with accuracy, sensitivity, and specificity values of 97.33%, 100%, and 94.87%, respectively. The F-scores of the three BP classifications were 97.29%, 97.39%, and 93.93%, respectively. The results of our proposed method demonstrated higher accuracy than a CNN method and regression methods such as the bagged tree, KNN, logistic regression, and AdaBoost tree methods. In future studies, we will use the

Stockwell transform to conduct frequency analysis of PPG signals [56]. In addition, increased sample sizes could be used to further improve the performance of BP classification based on PPG signals.

REFERENCES

[1] A. Al-Zaben, M. Fora, and A. Obaidat, "Detection of premature ventricular beats from arterial blood pressure signal," in *Proc. IEEE 4th Middle East Conf. Biomed. Eng. (MECBME)*, Tunis, Tunisia, Mar. 2018, pp. 17–19.

[2] A. Savkar, P. Khatate, and C. Patil, "Study on techniques involved in tourniqueteless blood pressure measurement using PPG," in *Proc. 2nd Int. Conf. Intell. Comput. Control Syst. (ICICCS)*, Madurai, India, Jun. 2018, pp. 170–172.

[3] G. Youssef, I. El Tebi, D. Osama, A. Shehahta, E. Baligh, Z. Ashour, and H. Gamal, "Familial history of hypertension as a predictor of increased arterial stiffness in normotensive offspring," *Egyptian Heart J.*, vol. 69, no. 1, pp. 37–44, Mar. 2017, doi: 10.1016/j.ehj.2016.07.003.

[4] A. Stojanova, S. Koceski, and N. Koceska, "Continuous blood pressure monitoring as a basis for ambient assisted living (AAL)—Review of methodologies and devices," *J. Med. Syst.*, vol. 43, no. 2, p. 24, Jan. 2019, doi: 10.1007/s10916-018-1138-8.

[5] C. Fischer and T. Penzel, "Continuous non-invasive determination of nocturnal blood pressure variation using photoplethysmographic pulse wave signals: Comparison of pulse propagation time, pulse transit time and RR-interval," *Physiol. Meas.*, vol. 40, no. 1, Nov. 2018, Art. no. 014001, doi: 10.1088/1361-6579/aaf298.

[6] F. Miao, Z. Liu, J. Liu, B. Wen, Q. He, and Y. Li, "Multi-sensor fusion approach for cuff-less blood pressure measurement," *IEEE J. Biomed, Health Inform.*, vol. 24, no. 1, pp. 79–91, Jan. 2020, doi: 10.1109/JBHI.2019.2901724.

[7] Z. Xu, J. Liu, X. Chen, Y. Wang, and Z. Zhao, "Continuous blood pressure estimation based on multiple parameters from eletrocardiogram and photoplethysmogram by Back-propagation neural network," *Comput. Ind.*, vol. 89, pp. 50–59, Aug. 2017, doi: 10.1016/j.compind.2017.04.003.

[8] H. Tjahjadi and K. Ramli, "Review of photoplethysmography based non-invasive continuous blood pressure methods," in *Proc. 15th Int. Conf. Qual. Res. (QiR), Int. Symp. Electr. Comput. Eng.*, Nusa Dua, Indonesia, Jul. 2017, pp. 173–178.

[9] S. Shimazaki, S. Bhuiyan, H. Kawanaka, and K. Oguri, "Features extraction for cuffless blood pressure estimation by autoencoder from photoplethysmography," in *Proc. 40th Annu. Int. Conf. IEEE Eng. Med. Biol. Soc. (EMBC)*, Honolulu, HI, USA, Jul. 2018, pp. 2857–2860.

[10] H. Tjahjadi and K. Ramli, "Variance analysis of photoplethysmography for blood pressure measurement," in *Proc. 4th Int. Conf. Electr. Eng., Comput. Sci. Informat. (EECSI)*, Yogyakarta, Indonesia, Sep. 2017, pp. 1–4.

[11] Y.-F. Fang, P.-W. Huang, M.-L. Chung, and B.-F. Wu, "A feature selection method for vision-based blood pressure measurement," in *Proc. IEEE Int. Conf. Syst., Man, Cybern. (SMC)*, Miyazaki, Japan, Oct. 2018, pp. 2158–2163.

[12] Y. Wu and S. Zhong, "Noninvasive blood pressure measurement based on photoplethysmography," in *Proc. Adv. Mech. Sci. Technol. Ind. Revolution (FZU)*, Singapore, Nov. 2018, pp. 121–131.

[13] S. Rajala, H. Lindholm, and T. Taipalus, "Comparison of photoplethysmogram measured from wrist and finger and the effect of measurement location on pulse arrival time," *Physiol. Meas.*, vol. 39, no. 7, May 2018, Art. no. 075010, doi: 10.1088/1361-6579/aac7ac.

[14] P. Su, X.-R. Ding, Y.-T. Zhang, J. Liu, F. Miao, and N. Zhao, "Long-term blood pressure prediction with deep recurrent neural networks," in *Proc. IEEE EMBS Int. Conf. Biomed. Health Informat. (BHI)*, Las Vegas, NV, USA, Mar. 2018, pp. 323–328.

[15] N. Apiwong-Ngam, S. Yarin, A. Ngamjarurojana, and S. Choopun, "Construction of blood pressure monitor using photoplethysmography calibrating with upper-arm blood pressure monitor," *J. Phys., Conf. Ser.*, vol. 1144, Dec. 2018, Art. no. 012152, doi: 10.1088/1742-6596/1144/1/012152.

[16] P. K. Lim, S.-C. Ng, N. H. Lovell, Y. P. Yu, M. P. Tan, D. Mccombie, E. Lim, and S. J. Redmond, "Adaptive template matching of photoplethysmogram pulses to detect motion artefact," *Physiol. Meas.*, vol. 39, no. 10, Sep. 2018, Art. no. 105005, doi: 10.1088/1361-6579/aadf1e.

[17] K. H. Blomqvist and L. Kärkkäinen, "Differential photoplethysmogram sensor with an optical notch filter shows potential for reducing motion artifact signals," *Biomed. Phys. Eng. Express*, vol. 4, no. 4, May 2018, Art. no. 047004, doi: 10.1088/2057-1976/aac57c.

[18] A. Dinh, L. Luu, and T. Cao, "Blood pressure measurement using finger ECG and photoplethysmogram for IoT," in *Proc. 6th Int. Conf. Develop. Biomed. Eng. (BME6)*, Vietnam, Jun. 2017, pp. 83–89.

[19] N. Bersano and H. Sanson, "Non-invasive blood pressure estimation from photoplethysmography signals using artificial neural networks," in *Proc. 20th Int. Conf. Adv. Commun. Technol. (ICACT)*, Chuncheon-si, South Korea, Feb. 2018, p. 1.

[20] H. Lim, B. Kim, G.-J. Noh, and S. Yoo, "A deep neural network-based pain classifier using a photoplethysmography signal," *Sensors*, vol. 19, no. 2, p. 384, Jan. 2019, doi: 10.3390/s19020384.

[21] Q. Zhang, X. Zeng, W. Hu, and D. Zhou, "A machine learning-empowered system for long-term motion-tolerant wearable monitoring of blood pressure and heart rate with Ear-ECG/PPG," *IEEE Access*, vol. 5, pp. 10547–10561, 2017, doi: 10.1109/access.2017.2707472.

[22] R. Raamat, K. Jagomagi, and J. Talts, "Continuous recording of the oscillometric mean arterial pressure by the differential servo system with two photoplethysmographic sensors," in *Proc. 8th IEEE Int. Conf. BioInform. BioEng.*, Athens, Greece, Oct 2008, pp. 1–4.

[23] G. Wang, M. Atef, and Y. Lian, "Towards a continuous non-invasive cuffless blood pressure monitoring system using PPG: Systems and circuits review," *IEEE Circuits Syst. Mag.*, vol. 18, no. 3, pp. 6–26, 3rd Quart., 2018, doi: 10.1109/mcas.2018.2849261.

[24] S. Datta, R. Banerjee, A. D. Choudhury, A. Sinha, and A. Pal, "Blood pressure estimation from photoplethysmogram using latent parameters," in *Proc. IEEE Int. Conf. Commun. (ICC)*, Kuala Lumpur, Malaysia, May 2016, pp. 1–7.

[25] L. Peter, N. Noury, and M. Cerny, "A review of methods for non-invasive and continuous blood pressure monitoring: Pulse transit time method is promising?" *IRBM*, vol. 35, no. 5, pp. 271–282, Oct. 2014, doi: 10.1016/j.irbm.2014.07.002.

[26] M. Kachuee, M. M. Kiani, H. Mohammadzade, and M. Shabany, "Cuffless blood pressure estimation algorithms for continuous health-care monitoring," *IEEE Trans. Biomed. Eng.*, vol. 64, no. 4, pp. 859–869, Apr. 2017, doi: 10.1109/tbme.2016.2580904.

[27] H. Jeong, M. Hayashi, M. Sekine, T. Tamura, M. Kido, K. Yamada, and Y. Ohno, "A study on estimating blood pressure during body postural change based on pulse transit time," in *Proc. IEEE Healthcare Innov. Conf. (HIC)*, Seattle, WA, USA, Oct. 2014, pp. 153–156.

[28] R. Kondo, M. S. Bhuiyan, H. Kawanaka, and K. Oguri, "Separate estimation of long- and short-term systolic blood pressure variability from photoplethysmograph," in *Proc. 36th Annu. Int. Conf. IEEE Eng. Med. Biol. Soc.*, Chicago, IL, USA, Aug. 2014, pp. 1851–1854.

[29] S.-C. Huang, P.-H. Hung, C.-H. Hong, and H.-M. Wang, "A new image blood pressure sensor based on PPG, RRT, BPTT, and harmonic balancing," *IEEE Sensors J.*, vol. 14, no. 10, pp. 3685–3692, Oct. 2014, doi: 10.1109/jsen.2014.2329676.

[30] A. D. Choudhury, R. Banerjee, A. Sinha, and S. Kundu, "Estimating blood pressure using Windkessel model on photoplethysmogram," in *Proc. 36th Annu. Int. Conf. IEEE Eng. Med. Biol. Soc.*, Chicago, IL, USA, Aug. 2014, pp. 4567–4570.

[31] M. Radha, K. De Groot, N. Rajani, C. C. P. Wong, N. Kobold, V. Vos, P. Fonseca, N. Mastellos, P. A. Wark, N. Velthoven, R. Haakma, and R. M. Aarts, "Estimating blood pressure trends and the nocturnal dip from photoplethysmography," *Physiol. Meas.*, vol. 40, no. 2, Jan. 2019, Art. no. 025006, doi: 10.1088/1361-6579/ab030e.

[32] A. Visvanathan, R. Banerjee, A. D. Choudhury, A. Sinha, and S. Kundu, "Smart phone based blood pressure indicator," in *Proc. 4th ACM MobiHoc Workshop Pervas. Wireless Healthcare-MobileHealth*, 2014, pp. 19–24.

[33] Y. Liang, Z. Chen, R. Ward, and M. Elgendi, "Photoplethysmography and deep learning: Enhancing hypertension risk stratification," *Biosensors*, vol. 8, no. 4, p. 101, Oct. 2018, doi: 10.3390/bios8040101.

[34] Y. Liang, Z. Chen, G. Liu, and M. Elgendi, "A new, short-recorded photoplethysmogram dataset for blood pressure monitoring in China," *Sci. Data*, vol. 5, Feb. 2018, Art. no. 180020, doi: 10.1038/sdata.2018.20.

[35] C. Orphanidou, "Quality assessment for the photoplethysmogram," in *Signal Quality Assessment in Physiological Monitoring*. New York, NY, USA: Springer, 2017, pp. 41–63, doi: 10.1007/978-3-319-68415-4_3.

[36] Y. Liang, M. Elgendi, Z. Chen, and R. Ward, "An optimal filter for short photoplethysmogram signals," *Sci. Data*, vol. 5, May 2018, Art. no. 180076, doi: 10.1038/sdata.2018.76.

[37] Č. Petar, "Skewness and kurtosis in function of selection of network traffic distribution," *Acta Polytechnica Hungarica*, vol. 7, no. 2, pp. 95–106, 2010.

[38] M. Elgendi, "Optimal signal quality index for photoplethysmogram signals," *Bioengineering*, vol. 3, no. 4, p. 21, Sep. 2016, doi: 10.3390/bioengineering3040021.
[39] M. B. Malarvili, L. Rankine, M. Mesbah, P. B. Colditz, and B. Boashash, "Heart rate variability characterization using a time-frequency based instantaneous frequency estimation technique," in *Proc. Kuala Lumpur Int. Conf. Biomed. Eng.*, Berlin, Germany, Dec. 2007, pp. 455–459.
[40] S. Nalband, C. Valliappan, A. A. Prince, and A. Agrawal, "Time-frequency based feature extraction for the analysis of vibroarthographic signals," *Comput. Electr. Eng.*, vol. 69, pp. 720–731, Jul. 2018, doi: 10.1016/j.compeleceng.2018.02.046.
[41] R. Romulus, "A comparison between instantaneous frequency estimation methods of frequency modulated signals covered with Gaussian noise," in *Proc. 10th Int. Symp. Electron. Telecommun.*, Timisoara, Romania, Nov. 2012, pp. 331–334.
[42] N. Sriraam and T. K. P. Shri, "Detection of alcoholic impact on visual event related potentials using beta band spectral entropy, repeated measures ANOVA and k-NN classifier," in *Proc. Int. Conf. Circuits, Controls, Commun. Comput. (I4C)*, Bangalore, India, Oct. 2016, pp. 1–4.
[43] A. Sarafnia, M. O. Ahmad, and M. N. S. Swamy, "A spectral entropy-based measure for performance evaluation of a first-order differential microphone array," in *Proc. IEEE 60th Int. Midwest Symp. Circuits Syst. (MWSCAS)*, Boston, MA, USA, Aug. 2017, pp. 863–866.
[44] Z. Cui and Y. Wang, "Deep bidirectional and unidirectional LSTM recurrent neural network for network-wide traffic speed prediction," pp. 22–25, Jul. 2018, *arXiv:1801.02143*. [Online]. Available: https://arxiv.org/abs/1801.02143
[45] F. P.-W. Lo, C. X.-T. Li, J. Wang, J. Cheng, and M. Q.-H. Meng, "Continuous systolic and diastolic blood pressure estimation utilizing long short-term memory network," in *Proc. 39th Annu. Int. Conf. IEEE Eng. Med. Biol. Soc. (EMBC)*, Seogwipo, South Korea, Jul. 2017, pp. 1853–1856.
[46] Y. Li, X. Li, Y. Zhang, W. Wang, M. Liu, and X. Feng, "Acoustic scene classification using deep audio feature and BLSTM network," in *Proc. Int. Conf. Audio, Lang. Image Process. (ICALIP)*, Shanghai, China, Jul. 2018, pp. 371–374.
[47] I. N. Yulita, M. I. Fanany, and A. M. Arymurthy, "Combining deep belief networks and bidirectional long short-term memory: Case study: Sleep stage classification," in *Proc. 4th Int. Conf. Electr. Eng., Comput. Sci. Informat. (EECSI)*, Yogyakarta, Indonesia, Sep. 2017, pp. 1–6.
[48] G. Liu and J. Guo, "Bidirectional LSTM with attention mechanism and convolutional layer for text classification," *Neurocomputing*, vol. 337, pp. 325–338, Apr. 2019, doi: 10.1016/j.neucom.2019.01.078.
[49] O. Yildirim, U. B. Baloglu, R.-S. Tan, E. J. Ciaccio, and U. R. Acharya, "A new approach for arrhythmia classification using deep coded features and LSTM networks," *Comput. Methods Programs Biomed.*, vol. 176, pp. 121–133, Jul. 2019, doi: 10.1016/j.cmpb.2019.05.004.
[50] Y. Liang, Z. Chen, R. Ward, and M. Elgendi, "Hypertension assessment via ECG and PPG signals: An evaluation using MIMIC database," *Diagnostics*, vol. 8, no. 3, p. 65, Sep. 2018, doi: 10.3390/diagnostics8030065.
[51] H. Shin and S. D. Min, "Feasibility study for the non-invasive blood pressure estimation based on PPG morphology: Normotensive subject study," *Biomed. Eng. Online*, vol. 16, no. 1, p. 10, Dec. 2017, doi. 10.1186/s12938-016-0302-y.
[52] T. Tamura, "Current progress of photoplethysmography and SPO2 for health monitoring," *Biomed. Eng. Lett.*, vol. 9, no. 1, pp. 21–36, Feb. 2019, doi: 10.1007/s13534-019-00097-w.
[53] N. Manshouri, M. Maleki, and T. Kayikcioglu, "An EEG-based stereoscopic research of the PSD differences in pre and post 2D&3D movies watching," *Biomed. Signal Process. Control*, vol. 55, Jan. 2020, Art. no. 101642.
[54] Q. Xie, G. Wang, Z. Peng, and Y. Lian, "Machine learning methods for real-time blood pressure measurement based on photoplethysmography," in *Proc. IEEE 23rd Int. Conf. Digit. Signal Process. (DSP)*, Shanghai, China, Nov. 2018, pp. 1–5.
[55] J. Brownlee. *'How to Scale Data for Long Short-Term Memory Networks in Python*. Accessed: Feb. 1, 2019. [Online]. Available: https://machinelearningmastery.com/how-to-scale-data-for-long-short-term-memory-networks-in-python
[56] R. Tripathy, M. R. Paternina, J. G. Arrieta, A. Zamora-Méndez, and G. R. Naik, "Automated detection of congestive heart failure from electrocardiogram signal using Stockwell transform and hybrid classification scheme," *Comput. Methods Programs Biomed.*, vol. 173, pp. 53–65, May 2019.

HENDRANA TJAHJADI (Member, IEEE) received the B.S. degree in electro-techniques and the M.S. degree in biomedical engineering from the Department of Electrical Engineering, Universitas Indonesia, Indonesia, in 2003 and 2015, respectively, where he is currently pursuing the Ph.D. degree. He has worked as a Biomedical Engineer for more than 24 years, with challenging work experience in bio-signals. His research interests include biomedical engineering and embedded systems.

KALAMULLAH RAMLI (Member, IEEE) received the master's degree (Hons.) in telecommunication engineering from the University of Wollongong, NSW, Australia, in 1997, and the Dr.-Ing. degree in computer networks from Universitaet Duisburg Essen, NRW, Germany, in 2003. He has been with the Universitas Indonesia (UI), since 1994, where he has been a Professor of computer engineering, since July 2009. He has published approximately 120 journal/conference papers and written seven books and chapters of books. His research interests include technology policy and management, embedded systems, data and network security, the Internet of Things, big data, and biomedical engineering.

HENDRI MURFI received the bachelor's degree in mathematics and the master's degree in computer science from the Universitas Indonesia and the Dr.rer.nat. degree from TU Berlin, Germany. He is currently serving as a Lecturer and a Researcher with the Data Science Group, Department of Mathematics, Universitas Indonesia. He performs research on machine learning with applications in topic modeling, sentiment analysis, recommender systems, and insurance.